ROUTING AND ACTION
MEMORANDUM

ROUTING

TO: (1) Electronics Division (Clark, William)

Report is available for review

(2) Proposal Files Proposal No.: 58141ELMUR.42

DESCRIPTION OF MATERIAL

CONTRACT OR GRANT NUMBER: W911NF-10-1-0524

INSTITUTION: University of Illinois - Urbana

PRINCIPAL INVESTIGATOR: Daniel Wasserman

TYPE REPORT: New Reprint

DATE RECEIVED: 8/28/13 4:11AM

PERIOD COVERED: through

TITLE: A calibration method for group V fluxes and impact of V/III flux ratio on the growth of InAs/InAsSb type-II superlattices by molecular beam epitaxy

ACTION TAKEN BY DIVISION

(x) Report has been reviewed for technical sufficiency and IS [x] IS NOT [ ] satisfactory.

( ) Material has been given an OPSEC review and it has been determined to be non sensitive and, except for manuscripts and progress reports, suitable for public release.

Approved by SSL\WILLIAM.CLARK on 1/22/15 5:03PM

ARO FORM 36-E

REPORT DOCUMENTATION PAGE

Form Approved OMB NO. 0704-0188

1. REPORT DATE (DD-MM-YYYY)	2. REPORT TYPE	3. DATES COVERED (From - To)
	New Reprint	-

4. TITLE AND SUBTITLE

A calibration method for group V fluxes and impact of V/III flux ratio on the growth of InAs/InAsSb type-II superlattices by molecular beam epitaxy

5a. CONTRACT NUMBER
W911NF-10-1-0524

5b. GRANT NUMBER

5c. PROGRAM ELEMENT NUMBER
611103

6. AUTHORS

Hua Li, Shi Liu, Oray O. Cellek, Ding Ding, Xiao-Meng Shen, Elizabeth H. Steenbergen, Jin Fan, Zhiyuan Lin, Zhao-Yu He, Qiang Zhang, Preston T. Webster, Shane R. Johnson, Lu Ouyang, David J. Smith,

5d. PROJECT NUMBER

5e. TASK NUMBER

5f. WORK UNIT NUMBER

7. PERFORMING ORGANIZATION NAMES AND ADDRESSES

University of Illinois - Urbana
Board of Trustees of the University of Illinois
1901 S First Street
Champaign, IL 61820 -7473

8. PERFORMING ORGANIZATION REPORT NUMBER

9. SPONSORING/MONITORING AGENCY NAME(S) AND ADDRESS(ES)

U.S. Army Research Office
P.O. Box 12211
Research Triangle Park, NC 27709-2211

10. SPONSOR/MONITOR'S ACRONYM(S)
ARO

11. SPONSOR/MONITOR'S REPORT NUMBER(S)
58141-EL-MUR.42

12. DISTRIBUTION AVAILIBILITY STATEMENT

Approved for public release; distribution is unlimited.

13. SUPPLEMENTARY NOTES

The views, opinions and/or findings contained in this report are those of the author(s) and should not contrued as an official Department of the Army position, policy or decision, unless so designated by other documentation.

14. ABSTRACT

A calibration method for group V fluxes is demonstrated for the growth of InAsxSb1?x alloys and strain-balanced InAs/InAsxSb1?x superlattices on GaSb substrates by molecular beam epitaxy for IR optoelectronic device applications. The structural and optical properties of these structures grown with varying V/III flux ratios are investigated using several characterization methods, including X-ray diffraction (XRD), photoluminescence (PL), and reflection high energy electron diffraction. Samples grown at 450 °C with Sb/In flux ratios from 1.0 to 2.0 and

15. SUBJECT TERMS

T2SLs

16. SECURITY CLASSIFICATION OF:			17. LIMITATION OF ABSTRACT	15. NUMBER OF PAGES	19a. NAME OF RESPONSIBLE PERSON
a. REPORT	b. ABSTRACT	c. THIS PAGE			Shun Chuang
UU	UU	UU	UU		19b. TELEPHONE NUMBER 217-721-3031

Report Title

A calibration method for group V fluxes and impact of V/III flux ratio on the growth of InAs/InAsSb type-II superlattices by molecular beam epitaxy

ABSTRACT

A calibration method for group V fluxes is demonstrated for the growth of InAsxSb1?x alloys and strain-balanced InAs/InAsxSb1?x superlattices on GaSb substrates by molecular beam epitaxy for IR optoelectronic device applications. The structural and optical properties of these structures grown with varying V/III flux ratios are investigated using several characterization methods, including X-ray diffraction (XRD), photoluminescence (PL), and reflection high energy electron diffraction. Samples grown at 450 °C with Sb/In flux ratios from 1.0 to 2.0 and As/In flux ratios from 1.2 to 2.5 lead to Sb mole fractions ranging from 0.078 to 0.34. High structural and optical quality superlattices for Sb mole fractions up to 0.34 are verified by XRD and low-temperature PL measurements. When varying both Sb mole fraction and period, superlattice structures are demonstrated with low-temperature emission wavelengths ranging from 3.6 to 7.1 ?m.

REPORT DOCUMENTATION PAGE (SF298)
(Continuation Sheet)

Continuation for Block 13

ARO Report Number 58141.42-EL-MUR
A calibration method for group V fluxes and impa ...

Block 13: Supplementary Note

Approved for public release; distribution is unlimited.

Journal of Crystal Growth 378 (2013) 145–149

Contents lists available at SciVerse ScienceDirect

Journal of Crystal Growth

journal homepage: www.elsevier.com/locate/jcrysgro

A calibration method for group V fluxes and impact of V/III flux ratio on the growth of InAs/InAsSb type-II superlattices by molecular beam epitaxy

Hua Li [a,b], Shi Liu [a,b], Oray O. Cellek [a,b], Ding Ding [a,b], Xiao-Meng Shen [b,c], Elizabeth H. Steenbergen [a,b], Jin Fan [b,d], Zhiyuan Lin [a,b], Zhao-Yu He [a,b], Qiang Zhang [a,b], Preston T. Webster [a,b], Shane R. Johnson [a,b], Lu Ouyang [a,b], David J. Smith [b,d], Yong-Hang Zhang [a,b,*]

[a] School of Electrical, Computer and Energy Engineering, Arizona State University, Tempe, AZ 85287, USA
[b] Center for Photonics Innovation, Arizona State University, Tempe, AZ 85287, USA
[c] School for Engineering of Matter, Transport and Energy, Arizona State University, Tempe, AZ 85287, USA
[d] Department of Physics, Arizona State University, Tempe, AZ 85287, USA

ARTICLE INFO

Available online 16 January 2013

Keywords:
A1. Characterization
A3. Molecular beam epitaxy
A3. Superlattices
B2. Semiconducting III–V materials

ABSTRACT

A calibration method for group V fluxes is demonstrated for the growth of $InAs_xSb_{1-x}$ alloys and strain-balanced $InAs/InAs_xSb_{1-x}$ superlattices on GaSb substrates by molecular beam epitaxy for IR optoelectronic device applications. The structural and optical properties of these structures grown with varying V/III flux ratios are investigated using several characterization methods, including X-ray diffraction (XRD), photoluminescence (PL), and reflection high energy electron diffraction. Samples grown at 450 °C with Sb/In flux ratios from 1.0 to 2.0 and As/In flux ratios from 1.2 to 2.5 lead to Sb mole fractions ranging from 0.078 to 0.34. High structural and optical quality superlattices for Sb mole fractions up to 0.34 are verified by XRD and low-temperature PL measurements. When varying both Sb mole fraction and period, superlattice structures are demonstrated with low-temperature emission wavelengths ranging from 3.6 to 7.1 μm.

1. Introduction

High performance infrared (IR) photodetectors are desirable for numerous commercial and defense applications. With a broad wavelength coverage (1–25 μm or even longer) and large absorption coefficient, HgCdTe has been the material of choice for mid-wavelength (MWIR, 3–5 μm) and long-wavelength (LWIR, 8–12 μm) IR photodetectors [1–3]. However, HgCdTe materials have several drawbacks such as mercury toxicity, lack of low-cost lattice-matched substrates, non-uniformity over large areas and challenging and high-cost epitaxial growth and device processing. Type-II superlattices (SLs) have been identified as one of the most promising types of alternative materials [4,5], and have been extensively studied for IR detector applications [6,7]. MWIR and LWIR focal plane arrays with excellent performance using InAs/(In)GaSb SLs have been demonstrated [8–13]. However, the minority carrier lifetime of the InAs/(In)GaSb SLs is limited by Shockley–Read–Hall (SRH) recombination and is significantly lower than that of HgCdTe [14,15]. Several other possible alternatives, namely Ga-free T2SLs, such as $InAs_{0.4}Sb_{0.6}/InAs_{1-x}Sb_x$ (with $x > 0.6$) SLs [16], and $InAs/InAs_{1-x}Sb_x$ SLs [17–20], were proposed many years ago for both LWIR and MWIR device applications. Recently, $InAs/InAs_{1-x}Sb_x$ SLs have attracted much attention for high-performance LWIR photodetectors applications due to their much simpler interface configurations, lower SRH recombination rates and longer carrier lifetimes [21–23]. One of the key challenges for the epitaxial growth of group-V alloys is the precise control of the alloy composition, which is a function of not only the growth temperature but also the ratios between group-III and group-V fluxes. To address the challenge, modulated molecular beam epitaxy method was introduced [24,25]. This paper reports a precise calibration method of group-V fluxes, which is reproducible and transferrable to any other MBE system, and a study of the structural and optical properties of infrared strain-balanced $InAs/InAs_{1-x}Sb_x$ type-II superlattices grown on GaSb substrates using this method with various V/III flux ratios by molecular beam epitaxy.

2. Experimental details

The epitaxial growth of the $InAs/InAs_{1-x}Sb_x$ SL samples are carried out in the III–V chamber of a VG V80H dual-chamber MBE system with In, Ga and Al group-III effusion cells and As and Sb

* Corresponding author at: School of Electrical, Computer and Energy Engineering, Arizona State University, Tempe, AZ 85287, USA. Tel.: +1 480 965 2562; fax: +1 480 965 0775.
E-mail address: yhzhang@asu.edu (Y.-H. Zhang).

0022-0248/$ - see front matter © 2013 Elsevier B.V. All rights reserved.
http://dx.doi.org/10.1016/j.jcrysgro.2012.12.144

group-V valved cracker cells. The crackers are operated at 990 °C producing group-V dimers or monomers [26]. Each effusion cell is equipped with a pneumatic shutter. The substrate temperature is monitored using an IRCON Modline3 infrared pyrometer. The growth parameters including shutter operation, effusion cell and substrate temperature ramps, and valve positioning are controlled by EMERALT software.

The growth rates for the group-III sources are calibrated before SL growth is initiated. The group-III beam-flux for each cell is measured using an ion gauge in terms of ion current as a function of cell thermocouple temperature. These curves are then converted to growth rates versus temperature based on a calibration point near the typical growth rate for a given binary material at its native lattice constant. The calibration curves are parameterized using an exponential fitting function that serves as a lookup function in the control software to set the effusion cell temperatures for the desired growth rates for each growth run. Each calibration function has a corresponding pre-factor that is adjusted to reflect the changes in the growth rate for different substrate lattice constants and the cell depletion using subsequent single temperature calibrations.

The AlAs and GaAs growth rates on GaAs are determined by growing GaAs/AlAs SL calibration samples and measuring the individual layer thicknesses using X-ray diffraction. The InAs growth rate on GaAs is determined by growing InGaAs/GaAs quantum wells and measuring the emission wavelength using photoluminescence (PL) spectroscopy. The growth rate for the GaSb and AlSb on GaSb is obtained based on GaAs and AlAs growth rates on GaAs and consideration of difference in the lattice constants. The growth rates of InAs and $InAs_{1-x}Sb_x$ on GaSb are obtained by multiplying the InAs and $InAs_{1-x}Sb_x$ constituent growth rates by the adjustment factors mentioned above, which take the strain effect into consideration.

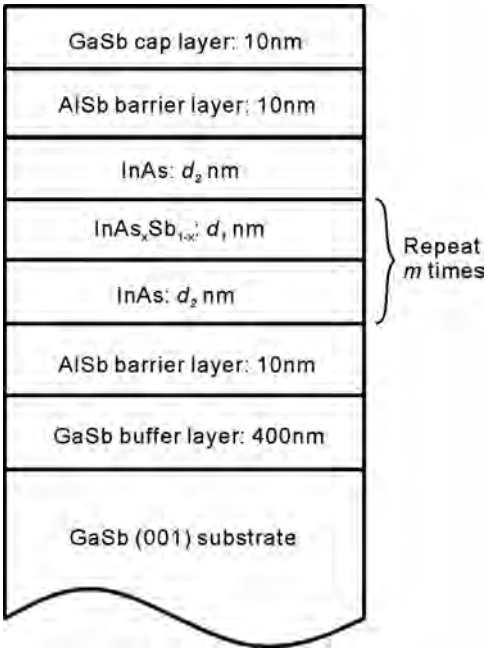

Fig. 1. Schematic diagram of the $InAs/InAs_{1-x}Sb_x$ superlattice sample layer structure.

The group-V fluxes are first measured in terms of ion current as a function of valve position with the group-V bulk zone set at a thermocouple temperature that provides the desired range of group-V fluxes over the operating range of the valve. The V/III flux ratios are then calibrated against the group-III fluxes by determining the minimum amount of group-V flux required to maintain a smooth group-V terminated growth surface for a given group-III growth rate at a given growth temperature. This calibration point is defined as the one-to-one V to III flux ratio (V/III=1) and the valve calibration curve is scaled proportionally to ion current to provide an effective group-V flux curve as a function of valve position. This procedure provides a calibration method that is reproducible and transferrable to any other MBE system. The V/III flux ratios are regularly calibrated during the growth campaigns and the temperatures of the group-V bulk zones are adjusted to compensate for the depletion of the bulk group-V materials. For example, this procedure results in a 0.1–0.2 °C per daily increase in the As bulk temperature when the system is growing arsenide materials. This calibration method has the advantage that the group-V flux curves can be expressed in the same units as those of the group-III growth rate curves, such as monolayers per second, as functions of valve position and bulk source temperature. Furthermore, in this approach, the group-V calibration curves rely on a precise growth condition rather than an arbitrary ion gauge current or pressure reading, which changes with time due to the coating of the ion gauge and varies from gauge to gauge and system to system, thus providing reproducible control of the group-V flux over time.

A schematic of the sample structure, consisting of an InAs/$InAs_{1-x}Sb_x$ SL sandwiched between two 10-nm AlSb barrier layers and a 10-nm GaSb cap layer is shown in Fig. 1. The samples are grown on 2″ epi-ready n-type GaSb (001) substrates. The surface oxide layer is thermally removed by slowly heating up the GaSb substrate under antimony flux until a clear, streaky (1×3) reflection-high-energy electron diffraction pattern is observed, which typically occurs at a temperature of ~530 °C. The substrate is kept at this temperature for 20 min before it is cooled down to 510 °C to grow a 400-nm GaSb buffer layer. During the SL growth, no growth interruption is introduced and a constant InAs growth rate of 9.15 nm/min on GaSb, derived from the InAs growth rate on InAs and one of the fixed As/In flux ratios listed in Table 1 is maintained while the Sb shutter is opened only for the $InAs_{1-x}Sb_x$ layers. The growth temperature, growth rate, and Sb/In flux ratio for GaSb buffer and capping layers are 510 °C, 9.1 nm/min and 2.0, respectively. The growth temperature is gradually ramped down to the SL growth temperature of 450 °C during the growth of the last 10-nm of the GaSb buffer layer, the first AlSb barrier layer and the first InAs layer, and ramped back to 510 °C during the growth

Table 1
Structure, growth condition, and X-ray diffraction (XRD) full width half maximum (FWHM) for various $InAs/InAs_{1-x}Sb_x$ type-II superlattice samples, where d_1 and d_2 are $InAs_{1-x}Sb_x$ and InAs layer thicknesses, respectively, and x is the Sb mole fraction.

Sample	d_1 (nm)	d_2 (nm)	Period number	Sb/III	As/III	Sb/As	x	XRD FWHM (arcsec)
A (B1760)	7.3	17	12	1.0	2.5	0.41	0.078	147
B (B1759)	7.3	17	12	2.0	2.5	0.81	0.145	184
C (B1761)	2.5	8.1	48	1.0	1.6	0.63	0.142	96.8
D (B1762)	2.5	8.1	91	1.0	1.2	0.83	0.255	38.2
E (B1766)	2.5	8.1	91	2.0	1.2	1.7	0.337	25.2
F (B1768)	2.5	8.1	91	2.4	1.2	2.0	0.334	28.8

of the last InAs layer and the second AlSb barrier layer prior to the growth of the final GaSb capping layer. Different designs and V/III flux ratios used for the growth of the InAs/$InAs_{1-x}Sb_x$ SL samples are summarized in Table 1.

High-resolution X-ray diffraction (XRD) measurements of the samples were performed using Cu K_1 radiation on a PANalytical X'Pert Pro Materials Research Diffractometer. The symmetric (004) and asymmetric (113) diffraction peaks were measured, from which the thicknesses of the SL constituent layers, the Sb composition in the $InAs_{1-x}Sb_x$ layers and full-width at half-maximum (FWHM) were determined. The results are listed in Table 1. Samples suitable for TEM examination in [110]-type projections were prepared by standard mechanical polishing, followed by argon-ion-milling at low energy (2–2.5 keV) with the sample held at liquid-nitrogen temperature to minimize any ion-beam damage. Electron micrographs were mostly recorded with a JEM-4000EX high-resolution electron microscope operated at 400 keV.

Low-temperature photoluminescence (PL) spectroscopy measurements were performed using a double-modulation method with a lock-in amplifier and a Fourier transform infrared spectrometer setup equipped with a liquid-nitrogen-cooled HgCdTe detector with a cut-off wavelength at 15 μm. A Janis ST-100 cryostat with a ZnSe window and a closed-cycled helium compressor were used to achieve 12 K during the measurements. The samples were optically pumped with a 780-nm semiconductor laser at an excitation density of $\sim$10 W/cm^2.

3. Results and discussion

Fig. 2 shows an example of the high-resolution (004) and (113) XRD patterns and simulations of sample E. Clear satellite peaks are observed and the FWHM of the zeroth-order SL peak is on the same order as that of the substrate, 20 arcsec, which is limited by the resolution of the XRD system. XRD FWHMs of all the samples, summarized in Table 1, indicate that when the Sb composition in the $InAs_{1-x}Sb_x$ layer is closer to 35%, the SLs are better strain-balanced and higher quality material is achieved. The lattice mismatch between the epilayer and the GaSb substrate is found to be -1.09×10^{-3}, indicating a small strain in this 1-μm-thick InAs/$InAs_{1-x}Sb_x$ SL. The separation between the substrate peak and the zeroth-order SL peak of the symmetric (004) diffraction gives the average lattice constant perpendicular to the (001) planes. Likewise, the average lattice constant perpendicular to the (113) planes is calculated from the asymmetric (113) diffraction peaks. With the assumption of tetragonal distortion in the epilayer, the average lattice spacing for the (110) planes is obtained, as well as the overall average Sb composition and average relaxation percentage of the InAs/$InAs_{1-x}Sb_x$ SL. The Sb composition x of the $InAs_{1-x}Sb_x$ layers is further derived taking into account the average growth duration of the $InAs_{1-x}Sb_x$ and InAs layers, or the monolayer ratio of $InAs_{1-x}Sb_x$ and InAs in the SLs. The analysis of the structural properties of a typical sample such as sample E shows that the Sb composition is 0.34 and that the SL film is coherently strained. The excellent structural quality of sample E is also confirmed by the cross-sectional electron micrograph shown in Fig. 3. Abrupt and smooth SL interfaces are clearly visible, with no growth defects observed in the micrograph.

The measured Sb compositions in the $InAs_{1-x}Sb_x$ layers versus Sb/In and As/In flux ratios are summarized in Fig. 4(a) and (b), respectively. For the InAs/$InAs_{1-x}Sb_x$ type-II SLs, higher Sb mole fractions and thicker periods lead to smaller SL band gaps, which is desirable for reaching longer detector cut-off wavelengths. As clearly shown in the figures, the incorporation of Sb increases

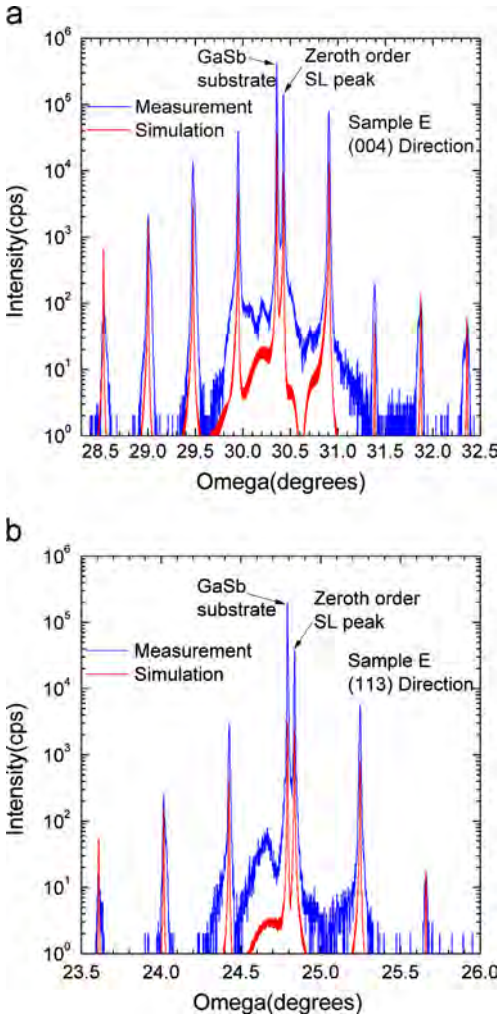

Fig. 2. High-resolution X-ray diffraction patterns (red curves) and simulations (blue curves) for sample E: (a) (004) scan and (b) (113) scan. (For interpretation of the references to color in this figure legend, the reader is referred to the web version of this article.)

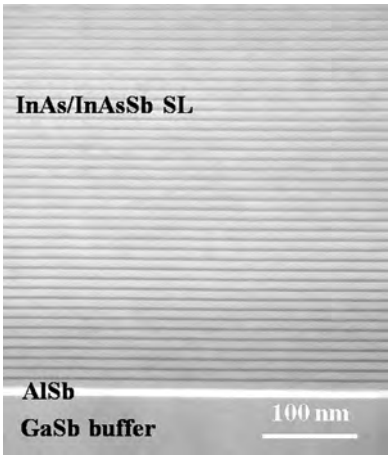

Fig. 3. Cross-sectional transmission electron micrograph of sample E showing excellent structural quality.

with either higher Sb/In or lower As/In flux ratios, and the increase of the Sb mole fraction saturates when Sb/In flux ratio becomes greater than 2. The saturation of Sb incorporation is expected at a growth temperature of 450 °C, since the sticking coefficient of Sb is much lower than that of As [27]. The same

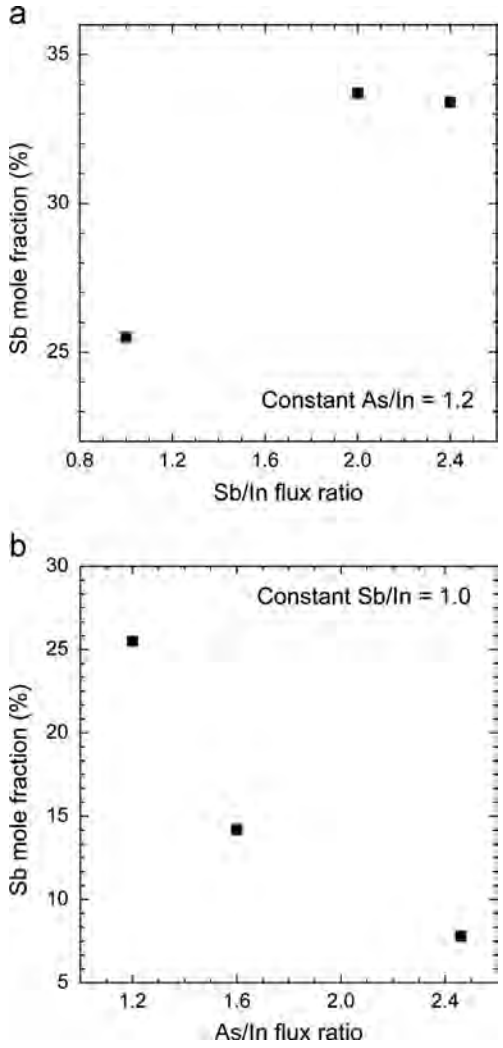

Fig. 4. Sb mole fractions of the $InAs_{1-x}Sb_x$ layers versus Sb/In flux ratios with As/In fixed at 1.2 as shown in (a) and As/In flux ratios with Sb/In fixed at 1.0 as shown in (b).

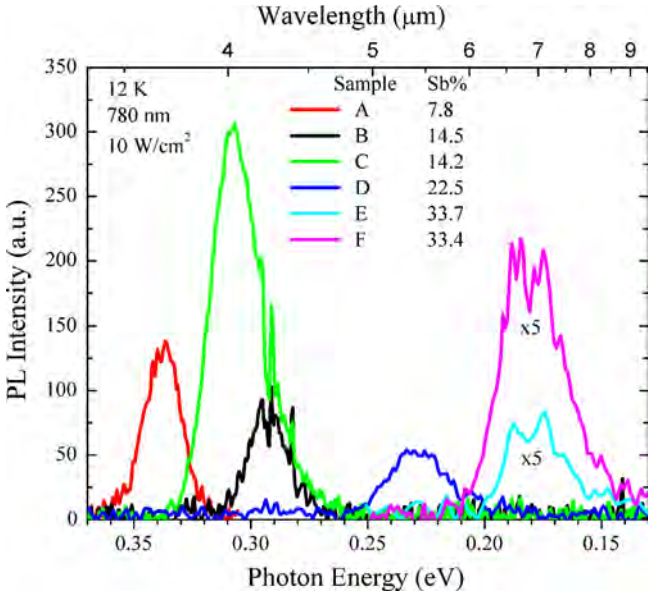

Fig. 5. Low-temperature (12 K) photoluminescence spectra for all InAs/$InAs_{1-x}Sb_x$ SL samples.

conclusion is obtained from the comparison of samples B and D. Even though these samples have similar Sb/As flux ratios of 0.81 and 0.83, the much higher Sb mole fraction (1.8 times) is achieved by reducing the total group-V overpressure by a factor of 0.5. However, the minimum As overpressure is limited by growth of the InAs layers because low As/In flux ratios lead to insufficient supply of As during the InAs layer growth. Furthermore, high Sb/In flux ratios can lead to unwanted Sb accumulating on the surface during the $InAs_{1-x}Sb_x$ growth and getting incorporated during the following InAs growth [28]. As a compromise, flux ratios of Sb/In=1.0–2.0 and As/In=1.2–2.5 provide a flux range that achieves good quality material and access to a wide range of wavelengths.

The low-temperature (12 K) PL spectra for all of these SL samples are shown in Fig. 5. These InAs/ $InAs_{1-x}Sb_x$ SLs can cover the range of wavelengths from 3.6 μm to 7.1 μm by using different V/III flux ratios. Higher Sb/III or lower As/III flux ratios lead to higher Sb compositions and larger type-II valance band offsets between InAs and $InAs_{1-x}Sb_x$, which then gives smaller effective bandgap of the SL.

4. Conclusions

In conclusion, a reproducible and transferrable method is proposed and demonstrated for the calibration of group-V fluxes during molecular beam epitaxy. The structural and optical properties of strain-balanced InAs/$InAs_{1-x}Sb_x$ type-II superlattices grown on GaSb substrates using this method with various V/III flux ratios are studied. The mole fraction of Sb incorporated into the $InAs_{1-x}Sb_x$ layers during growth increases when either the As/In flux ratio is decreased or the Sb/In flux ratio is increased up to a point when additional Sb no longer incorporates at a growth temperature of 450 °C. The realization of superlattices with high structural quality and precise strain balance is confirmed by XRD measurements and TEM structural studies. High quality type-II InAs/$InAs_{1-x}Sb_x$ SL structures with transition energies covering the wavelength range from 3.6 to 7.1 μm are achieved using growth temperatures around 450 °C and V/III flux ratios over the range of Sb/In=1.0–2.0 and As/In=1.2–2.5.

Acknowledgments

The authors are grateful for the support of a MURI W911NF-10-1-0524 (administered by U.S. Army Research Office and monitored by William W. Clark) and an AFOSR Grant FA9550-10-1-0129 (monitored by Kitt Reinhardt), and gratefully acknowledge use of facilities in the John M. Cowley Center for High Resolution Electron Microscopy at Arizona State University.

References

[1] P. Norton, Opto-Electronics Review 10 (2002) 159.
[2] M.B. Reine, Photovoltaic detectors in HgCdTe, in: P. Capper, C.T. Elliott (Eds.), Infrared Detectors and Emitters: Materials and Devices, Kluwer, Boston, MA, 2000.
[3] S.M. Johnson, A.A. Buell, M.F. Viela, J.M. Peterson, J.B. Varesi, M.D. Newton, G.M. Venzor, R.E. Bomfreund, W.A. Radford, E.P.G. Smith, J.P. Rosbeck, T.J. De Lyon, J.E. Jensen, V. Nathan, Journal of Electronic Materials 33 (2004) 526.
[4] L. Esaki, R. Tsu, IBM Journal of Research and Development 14 (1970) 61.
[5] G. Sai-Halasz, R. Tsu, L. Esaki, Applied Physics Letters 30 (1977) 651.
[6] D.L. Smith, C. Mailhot, Applied Physics Letters 62 (1987) 2545.
[7] P.M. Young, C.H. Grein, H. Ehrenheich, R.H. Miles, Journal of Applied Physics 74 (1993) 4774.
[8] S.B. Rafol, A. Soibel, A. Khoshakhlagh, J. Nguyen, J.K. Liu, J.M. Mumolo, S.A. Keo, L. Hoglund, D.Z. Ting, S.D. Gunapala, IEEE Journal of Quantum Electronics 48 (2012) 878.
[9] M. Sundaram, A. Reisinger, R. Dennis, K. Patnaude, D. Burrows, J. Bundas, K. Beech, R. Faska, Infrared Physics & Technology 54 (2011) 243.

[10] M. Razeghi, D. Hoffman, B.-M. Nguyen, P.-Y. Delaunay, E.K.-W. Huang, M.Z. Tidrow, V. Nathan, Proceedings of the IEEE 97 (2009) 1056.
[11] H.S. Kim, E. Plis, J.B. Rodriguez, G.D. Bishop, Y.D. Sharma, L.R. Dawson, S. Krishna, J. Bundas, R. Cook, D. Burrows, R. Dennis, K. Patnaude, A. Reisinger, M. Sundaram, Applied Physics Letters 92 (2008) 183502.
[12] R. Rehm, M. Walther, J. Schmitz, J. Fleissner, F. Fuchs, J. Ziegler, W. Cabanski, Opto-Electronics Review 14 (2006) 19.
[13] I. Vurgaftman, C.L. Canedy, E.M. Jackson, J.A. Nolde, C.A. Affouda, E.H. Aifer, J.R. Meyer, A. Hood, A.J. Evans, W.T. Tennant, Optical Engineering 50 (2011) 061007.
[14] B.C. Connelly, G.D. Metcalfe, H. Shen, M. Wraback, Applied Physics Letters 97 (2010) 251117.
[15] D. Donetsky, G. Belenky, S. Svensson, S. Suchalkin, Applied Physics Letters 97 (2010) 052108.
[16] G.C. Osbourn, Journal of Vacuum Science & Technology B 2 (1984) 176.
[17] Y.-H. Zhang, Applied Physics Letters 66 (1995) 118.
[18] A.Y. Lew, E.T. Yu, Y.-H. Zhang, Journal of Vacuum Science & Technology B 14 (1996) 2940.
[19] Y.-H. Zhang, in: M.O. Manasreh (Ed.), Optoelectronic Properties of Semiconductors and Superlattices: Antimonide-Related Strained-Layer Heterostructures, vol. 3, Gordon, Breach, 1997.
[20] C.H. Grein, M.E. Flatte, H. Ehrenreich, in: Proceedings of the Third International Symposium on Long Wavelength Infrared Detectors and Arrays: Physics and Applications III, 8–13 October 1995, Chicago, Illinois, p. 211.
[21] Y. Huang, J.-H. Ryou, R.D. Dupuis, V.R. D'Costa, E.H. Steenbergen, J. Fan, Y.-H. Zhang, A. Petschke, M. Mandl, S.-L. Chuang, Journal of Crystal Growth 314 (2011) 92.
[22] E.H. Steenbergen, Y. Huang, J.-H. Ryou, L. Ouyang, J.-J. Li, D.J. Smith, R.D. Dupuis, Y.-H. Zhang, Applied Physics Letters 99 (2011) 071111.
[23] E.H. Steenbergen, B.C. Connelly, G.D. Metcalfe, H. Shen, M. Wraback, D. Lubyshev, Y. Qiu, J.M. Fastenau, A.W.K. Liu, S. Elhamri, O.O. Cellek Y.-H. Zhang, Applied Physics Letters 99 (2011) 251110.
[24] Y.-H. Zhang, D.H. Chow, Applied Physics Letters 65 (1994) 3239.
[25] Y.-H. Zhang, Journal of Crystal Growth 150 (1995) 838.
[26] P.D. Brewer, D.H. Chow, R.H. Miles, Journal of Vacuum Science & Technology B 14 (1996) 2335.
[27] S. Baba, H. Horita, A. Kinbara, Journal of Applied Physics 49 (1978) 3632.
[28] H. Miyoshi, R. Suzuki, H. Amano, Y. Horikoshi, Journal of Crystal Growth 237 (2002) 1519.